

# Nuclear dynamics in the EMC effect at Next to Next to Leading order

S.Atashbar Tehrani<sup>1,2a</sup> and H. Mouji<sup>3</sup>

<sup>1</sup> Department of Physics, Yazd Branch, Islamic Azad University, Yazd, Iran

<sup>2</sup> School of Particles and Accelerators, Institute for Research in Fundamental Sciences (IPM), P.O.Box 19395-5531, Tehran, Iran

<sup>3</sup> Payame Noor University Bushehr, Iran

Received: July 25, 2021/ Revised version: date

**Abstract.** We study in details the parameterizations of the nuclear parton distributions at the next-to-next-to-leading order (NNLO) of  $\alpha_s$ . In low  $x$  and  $Q_0^2$ , we observe negative gluon distribution at this order which signals the saturation condition or the quark-gluon plasma condition. Our study also shows the gluon distribution at (NNLO) is less than next-to-leading order (NLO) of  $\alpha_s$ , and the sea quark distribution at (NNLO) is larger than (NLO)

**PACS.**

25.30.Mr Muon-induced reactions (including the EMC effect) –

13.85.Qk Inclusive production with identified leptons, photons, or other nonhadronic particles –

12.39.-x Phenomenological quark models –

14.65.Bt Light quarks

## 1 Introduction

Deep Inelastic Scattering (DIS) provides a tool for probing the quark momentum distribution in the nucleons and in the nuclei. Since the first indications that the DIS structure functions measured in the charged-lepton scattering off the nuclei differ significantly from those measured in the isolated nucleons, there has been a continuous interest in fully understanding the microscopic mechanism responsible in nuclei. This phenomena called EMC effect which was discovered surprisingly in 1983 [1]. After then it was being investigated how it affects the momentum distribution of quarks in nuclei. We indicate that the parton distributions in nuclei are not simply as the parton densities in the nucleons. In addition to the most commonly analyzed data sets for deep-inelastic scattering of charged leptons off nuclei, we also analysis the Drell-Yan di-lepton production. At low values of the Bjorken scaling variable  $x$  the ratio is  $R = F_2^A/F_2^D < 1$ . At medium values of  $x$ ,  $R$  drops from 1 to values as low as 0.8 and at large  $x$  it reaches values larger than 1. While the latter feature can be quantitatively explained by the smearing of the parton distribution functions arising from the momentum distribution of nucleons in nuclei, the former one is accounted for by including the effect of nuclear shadowing. This Phenomena divided to 4 region in  $x \leq 0.05$  we have shadowing

effect. The interval  $0.05 \leq x \leq 0.3$  belongs to antishadowing region. In  $x = 0.6 \sim 0.7$  we encounter with EMC effect and for large  $x$  we have fermimotion. While extended experimental and theoretical efforts were put into studies of the origin of the EMC effect, an acceptable explanation has yet to be found. One of the major goals of Quantum Chromo Dynamics (QCD) is the particular investigation of the parton distribution of the proton and nuclei which for the first time has been observed by the European Muon collaboration (EMC). Deep inelastic scattering (DIS) experiment which have been performed by NMC, SLAC, NMC, FNAL, BCDMS, HERMES and JLAB groups [6, 7, 8, 9, 10, 11, 12, 13, 14, 15, 16, 17, 18, 19, 20, 21, 22] confirm the specific feature of nuclear reaction at certain region of  $x$ -Bjorken variable which was first observed by EMC collaborations. This specific feature has also been seen in Drell-Yan cross section ratios [23, 24]. In this paper we calculate the nuclear parton distribution functions (NPDFs), using the global analysis of experimental data, taking into account the ratio of the structure function,  $F_2^A/F_2^{A'}$ , and Drell-Yan cross-section ratios  $\sigma_{DY}^A/\sigma_{DY}^{A'}$  by employing the QCD-PEGASUS-package [25].

This paper consists of the following sections. In Sec.1, A formalism to establish an analysis method to parameterize the experimental data is introduced. In Sec. 2 we embark this analysis to follow our calculations. We give our calculations in Sec. 3. The Hessian method is discussed in Sec. 4 and finally results are given in Sec. 5.

Send offprint requests to:

<sup>a</sup> Present address: atashbar@ipm.ir

## 2 Formalism

In order to calculate the parton distribution in nuclear media, we need first the parton distributions in a free proton. We then use a PDFs set which have been parameterized at the input scale  $Q_0^2 = 2 \text{ GeV}^2$  with the following standard form, quoted from [26]:

$$xq(x, Q_0^2) = A_q x^{\alpha_q} (1-x)^{\beta_q} (1 + \gamma_q x^{0.5} + \eta_q x) . \quad (1)$$

The PDFs in above are used as the valance quark distributions  $xu_v$ ,  $xd_v$ , the anti-quark distributions  $x\bar{s} = \frac{x(\bar{u}+\bar{d}+\bar{s})}{3}$ ,  $x\Delta = x(\bar{d}-\bar{u})$ , and gluon distribution,  $xg$ . In this paper a comparison between the results of used model in [26] and the experimental groups BCDMS, H1, NMC, SLAC and ZEUS at an input scale of  $Q_0^2 = \mu_{NLO}^2 = 2 \text{ GeV}^2$  has been done.

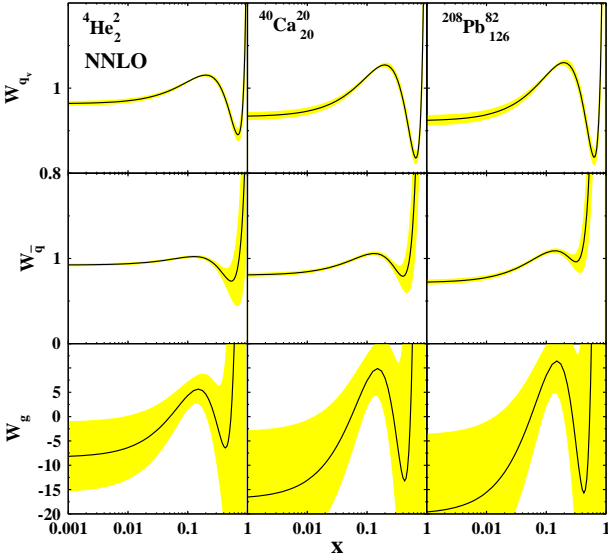


**Fig. 1.** The weight functions for  $^4\text{He}$ ,  $^{40}\text{Ca}$  and  $^{208}\text{Pb}$  nuclei at  $Q_0^2 = 2 \text{ GeV}^2$ .

We know the NPDFs are provided by a number of parameters at a fixed  $Q^2$  which are normally denoted by  $Q_0^2$ . The NPDFs are related to PDFs in free proton and for this purpose nucleonic PDFs are multiplied by a weight function  $w_i$ :

$$f_i^A(x, Q_0^2) = w_i(x, A, Z) f_i(x, Q_0^2) . \quad (2)$$

The parameters in weight function are obtained by a  $\chi^2$  analysis procedure which are dependent on  $x$  Bjorken variable,  $A$  (mass number) and  $Z$  (atomic number).

Here we follow the analysis given by [27, 28, 29, 30, 31, 32, 33] and assume the functional form in below for the weight function in Eq. (2):

$$w_i(x, A, Z) = 1 + \left(1 - \frac{1}{A^\alpha}\right) \frac{a_i(A, Z) + b_i(A)x + c_i(A)x^2 + d_i(A)x^3}{(1-x)^{\beta_i}} . \quad (3)$$

Combining the weight function in Eq. (3) with PDFs in Eq. (1), will yield us us NPDFs as in what follows:

$$\begin{aligned} u_v^A(x, Q_0^2) &= w_{u_v}(x, A, Z) \frac{Z u_v(x, Q_0^2) + N d_v(x, Q_0^2)}{A} , \\ d_v^A(x, Q_0^2) &= w_{d_v}(x, A, Z) \frac{Z d_v(x, Q_0^2) + N u_v(x, Q_0^2)}{A} , \\ \bar{u}^A(x, Q_0^2) &= w_{\bar{u}}(x, A, Z) \frac{Z \bar{u}(x, Q_0^2) + N \bar{d}(x, Q_0^2)}{A} , \\ \bar{d}^A(x, Q_0^2) &= w_{\bar{d}}(x, A, Z) \frac{Z \bar{d}(x, Q_0^2) + N \bar{u}(x, Q_0^2)}{A} , \\ s^A(x, Q_0^2) &= w_{\bar{s}}(x, A, Z) s(x, Q_0^2) , \\ g^A(x, Q_0^2) &= w_g(x, A, Z) g(x, Q_0^2) . \end{aligned} \quad (4)$$

In the first four equations,  $Z$  term as atomic number indicates the number of protons and the  $(N = A - Z)$  term indicate the number of neutrons in in nuclei while the  $SU(3)$  symmetry is apparently broken there. If the number of protons and neutrons in a nuclei are equal to each other (iso-scalar nuclei) such as  $^2\text{D}$ ,  $^4\text{He}$ ,  $^{12}\text{C}$  and  $^{40}\text{Ca}$  nuclei, the valance quarks  $u_v^A$  and  $d_v^A$  and  $\bar{u}^A$  and  $\bar{d}^A$  would have similar distributions. In the case that  $Z$  and  $A$  numbers are not equal in the nuclei, it can be concluded that anti-quark distributions ( $\bar{u}^A$ ,  $\bar{d}^A$ ,  $\bar{s}^A$ ) in the nuclei would not be equal to each other [33, 34, 35]. For the strange quark distributions in the nuclei some research studies are still being done [36] but we assume the common case in which it is assumed ( $s = \bar{s}$ ). In Eq. (3) we take  $\alpha = 1/3$  as in [37] considering nuclear volume and surface contributions. In addition there are three constraints for the parameters which are existed in Eq. (3) namely the nuclear charge  $Z$ , baryon number (mass number)  $A$  and momentum conservation [27, 28, 33, 38] as in following:

$$\begin{aligned} Z &= \int \frac{A}{3} [2u_v^A - d_v^A] (x, Q_0^2) dx , \\ 3 &= \int [u_v^A + d_v^A] (x, Q_0^2) dx , \\ 1 &= \int x [u_v^A + d_v^A + 2 \{ \bar{u}^A + \bar{d}^A + \bar{s}^A \} \\ &\quad g^A] (x, Q_0^2) dx . \end{aligned} \quad (5)$$

## 3 Overview of the available experimental data

In Table 1, we listed a number of the data which has been prepared by different experimental groups for the

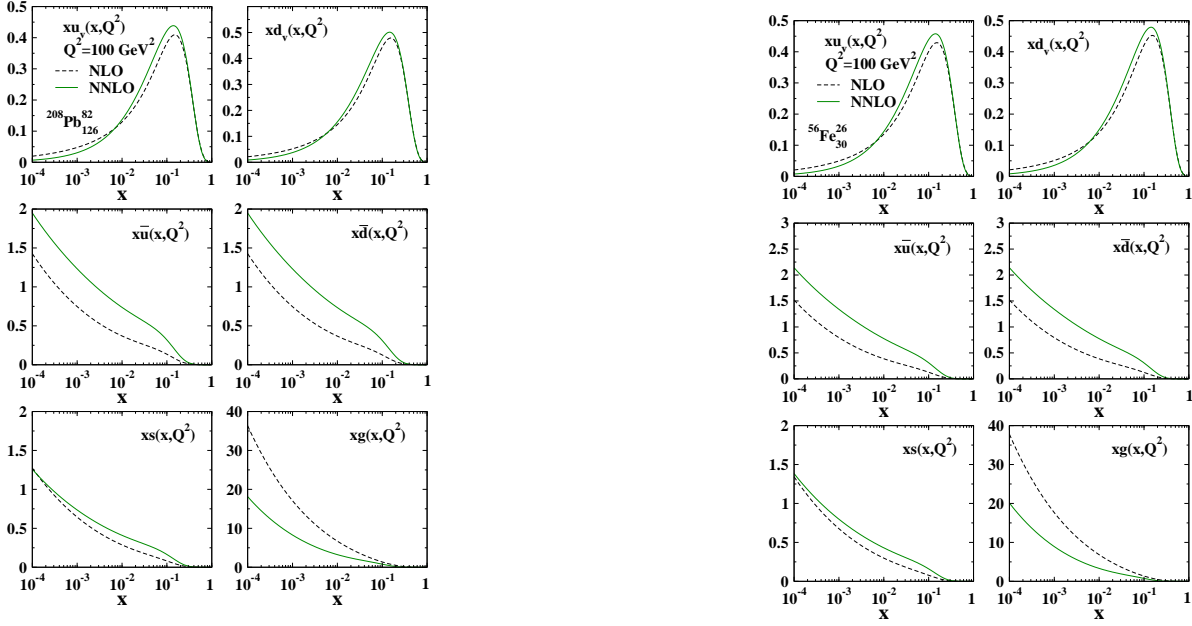


**Fig. 2.** Parton distribution for Lead and Iron at  $Q^2=100 \text{ GeV}^2$  in NNLO and its comparison with the NLO results. [33].

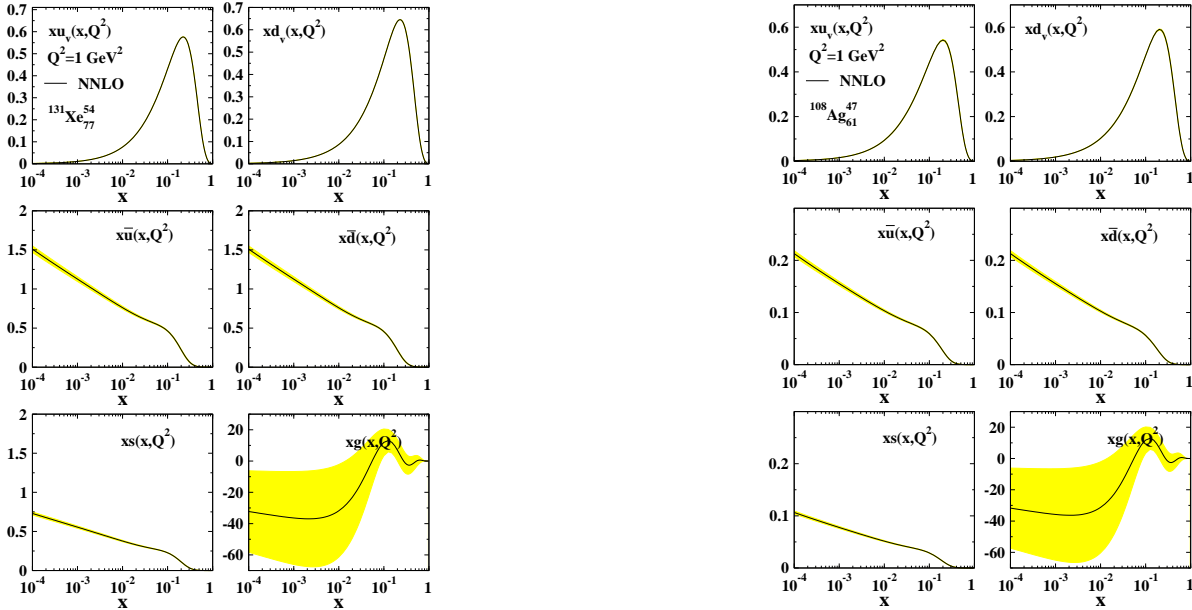


**Fig. 3.** Parton distribution for Xenon and Silver at  $Q^2 = 1 \text{ GeV}^2$  in NNLO approximation including the error band.

$F_2^A/F_2^D$  ratio. In this ratio the numerator is denoting the structure function of a nuclei and denominator is representing the structure function of Deuterium. The total number of data for the ratio in which the numerator includes nuclei like Helium ( $He$ ), Lithium ( $Li$ ) and etc. is equal to 1079. In Table the number of  $F_2^A/F_2^{A'}$  ratio for  $Be/C$ ,  $Al/C$ ,  $Ca/C$ ,  $Fe/C$ ,  $Sn/C$ ,  $Pb/C$ ,  $C/Li$  is 308. For Drell-Yan cross section ratios in table 1 the number of data is equal to 92 while the related ratio are  $C/D$ ,

$Ca/D$ ,  $Fe/D$ ,  $W/D$ ,  $Fe/Be$  and  $W/Be$ . In the employed analysis the total number of data is 1479. The interval range of  $Q^2$  values is  $Q^2 \geq 1 \text{ GeV}^2$  and the smallest value for Bjorken variable  $x$  is equal to 0.0055.

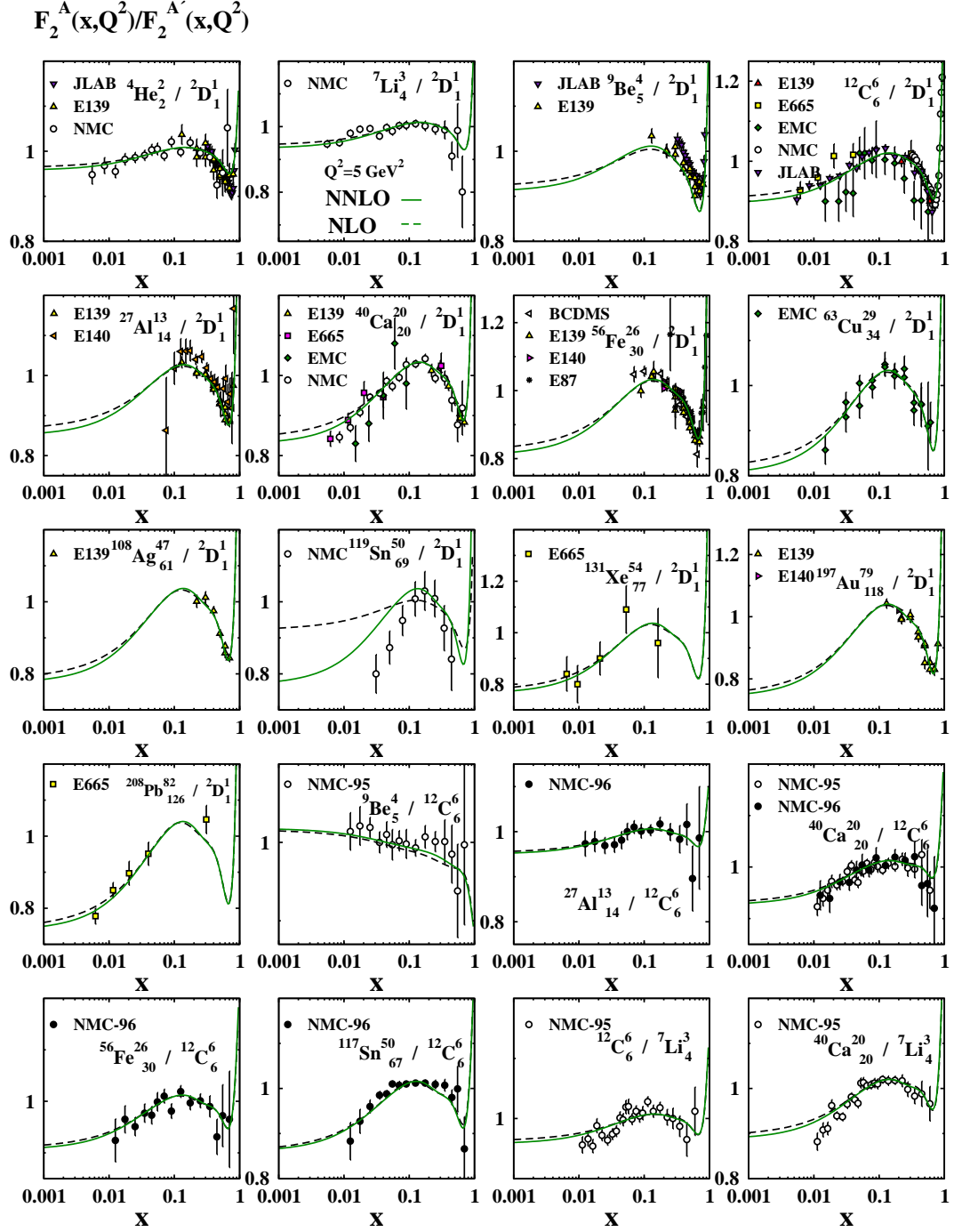


**Fig. 4.** EMC ratio for several nuclei at  $Q^2 = 5 \text{ GeV}^2$ , in NNLO approximation and its comparison with the NLO approximation [33] .

#### 4 The analysis of $\chi^2$ value

We use the MINUIT fitting package [39] to fit the experimental data, including the structure function  $F_2^A/F_2^{A'}$  and Drell-Yan cross section ratios.

The optimized value of total  $\chi^2$  is defined by

$$\chi^2 = \sum_j \frac{(R_j^{data} - R_j^{theo})^2}{(\sigma_j^{data})^2} . \quad (6)$$

This relation yield us the proper parameters for NPDFs. Here  $R_j^{data}$  indicates the experimental values for  $F_2^A/F_2^{A'}$  or  $\sigma_{DY}^A/\sigma_{DY}^{A'}$  ratio and  $R_j^{theo}$  is denoting the theoretical

Nucleus	Experiment	#of data	Reference
$(F_2^A/F_2^D)$			
He/D	SLAC-E139	18	[18]
	NMC-95	17	[6]
Li/D	NMC-95	17	[6]
	NMC-95	179	[6]
Be/D	SLAC-E139	17	[7]
C/D	EMC-88	9	[13]
	EMC-90	5	[18]
SLAC-E139	SLAC-E139	7	[7]
	NMC-95	17	[6]
FNAL-E665	FNAL-E665	5	[15]
	JLAB-E03-103	103	[16]
C/D(Q <sup>2</sup> dep.)	NMC-95	191	[6]
	BCDMS-85	9	[19]
N/D	HERMES-03	153	[22]
Al/D	SLAC-E49	18	[8]
	SLAC-E139	17	[7]
Ca/D	EMC-90	5	[18]
	NMC-95	16	[6]
SLAC-E139	SLAC-E139	7	[18]
	FNAL-E665	5	[15]
Fe/D	SLAC-E87	14	[9]
	SLAC-E139	23	[7]
SLAC-E140	SLAC-E140	10	[10]
	BCDMS-87	10	[11]
Cu/D	EMC-93	19	[12]
Kr/D	HERMES-03	144	[22]
Ag/D	SLAC-E139	7	[7]
Sn/D	EMC-88	8	[13]
Xe/D	FNAL-E665-92	5	[14]
Au/D	SLAC-E139	18	[7]
	SLAC-E140	1	[10]
Pb/D	FNAL-E665-95	5	[15]
$(F_2^A/F_2^{A'})$			
Be/C	NMC-96	15	[21]
Al/C	NMC-96	15	[21]
Ca/C	NMC-96	24	[6]
	NMC-96	15	[21]
Fe/C	NMC-96	15	[21]
Sn/C	NMC-96	146	[21]
	NMC-96	15	[21]
Pb/C	NMC-96	15	[21]
C/Li	NMC-95	24	[6]
Ca/Li	NMC-95	24	[6]
$(\sigma_{DY}^A/\sigma_{DY}^{A'})$			
C/D	FNAL-E772-90	9	[24]
Ca/D	FNAL-E772-90	9	[24]
Fe/D	FNAL-E772-90	9	[24]
W/D	FNAL-E772-90	9	[24]
Fe/Be	FNAL-E866/NuSea	28	[23]
W/Be	FNAL-E866/NuSea	28	[23]
Total		1479	

**Table 1.** Different experimental results for the  $F_2^A/F_2^D$ ,  $F_2^A/F_2^{A'}$  and  $\sigma_{DY}^A/\sigma_{DY}^{A'}$  ratio at  $Q^2 \geq 1.0$  GeV<sup>2</sup>. Number of data points and the related references are also listed.

result for the parameterized NPDFs. In our calculations, we take  $Q_0^2 = 2$  GeV<sup>2</sup> [26] and the  $\chi^2$  analysis is done, based on the DGLAP evolution equations [25]. Our calculations are done in the next-next-to-leading (NNLO) approximation in which the modified minimal subtraction scheme ( $\overline{MS}$ ) is used [40].

Therefore the nuclei structure function is written as in following:

$$F_2^A(x, Q^2) = \sum_{i=u,d,s} e_i^2 x [1 + a_s C_q^1(x) + a_s^2 C_q^2(x)] \otimes (q_i^A + \bar{q}_i^A) + \frac{1}{2f} (a_s C_g^1(x) + a_s^2 C_g^2(x)) \otimes xg. \quad (7)$$

In this equation,  $C_{q,g}^{1,2}$  are wilson coefficient in NLO and NNLO approximation [41,42] and the symbol  $\otimes$  denotes the convolution integral:

$$f(x) \otimes g(x) = \int_x^1 \frac{dy}{y} f\left(\frac{x}{y}\right) g(y). \quad (8)$$

We employ the CERN program library MINUIT to minimize the  $\chi^2$  value. Following that an error analysis can be done, using the Hessian matrix. The NPDFs uncertainties are estimated, using the Hessian matrix as in following:

$$[\delta f^A(x)]^2 = \Delta\chi^2 \sum_{i,j} \left( \frac{\partial f^A(x, \xi)}{\partial \xi_i} \right)_{\xi=\hat{\xi}} H_{ij}^{-1} \left( \frac{\partial f^A(x, \xi)}{\partial \xi_j} \right)_{\xi=\hat{\xi}}, \quad (9)$$

where  $H_{ij}$  is the Hessian matrix,  $\xi_i$  is a quantity refereing to the parameters which exist in NPDFs and  $\hat{\xi}$  indicates the amount of the parameter which makes an extremum value for the related derivative[33].

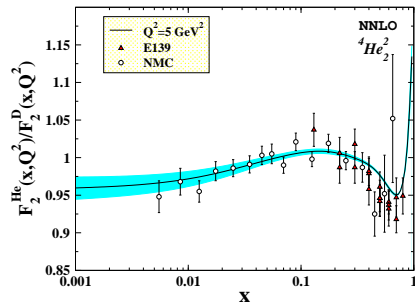


**Fig. 5.** EMC effect for Helium at  $Q^2 = 5$  GeV<sup>2</sup>, in NNLO approximation including the error band.

## 5 Results

In our analysis we use the weight function method as in Ref. [33]. However in this analysis we assume that the coefficients in Eq. (3) depend on nuclear mass number,  $A$ .

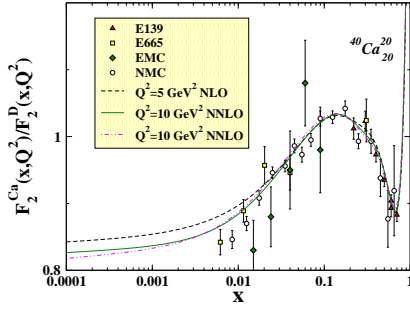


**Fig. 6.** EMC effect for Calcium at  $Q^2 = 5, 10 \text{ GeV}^2$ , in NNLO approximation and its comparison with the NLO approximation [33].

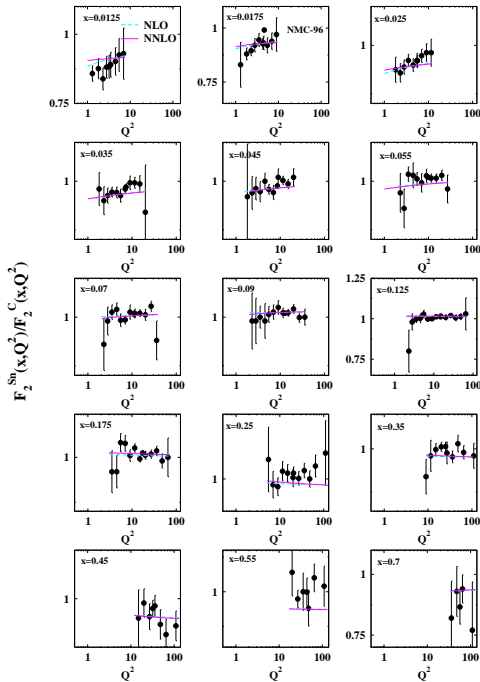


**Fig. 7.**  $Q^2$  dependence of  $F_2^{Sn}/F_2^C$  [21] in comparison with the NNLO and NLO approximations [33].

In our analysis which is done in the NNLO approximation, we get to  $\chi^2/D.O.F = 1614.90/1462 = 1.1046$ . The number of the data points for the nuclei and Drell-Yan ratios is totally 1479. The number of parameters which is used in our fitting procedure is equal to 17. In Fig. 1 we depict the weight functions for the Helium, Calcium and Lead nuclei at initial value  $Q_0^2 = 2 \text{ GeV}^2$ . In this figure, the uncertainties are indicated by the bands. We extract the NPDFs for Lead and Iron nuclei at  $Q^2 = 100 \text{ GeV}^2$  in NNLO model and compare it with NLO result in [33] Fig. 2. These figure show that the sea quark distribution in NNLO approximation is greater than NLO and also the gluon distribution in NNLO approximation is less than NLO approximation.

In Fig. 3 we plot the parton distributions in  $Q_0^2 = 2 \text{ GeV}^2$  with error bar for Xenon and Silver. In this Figure, we have negative distribution for gluon. We compare

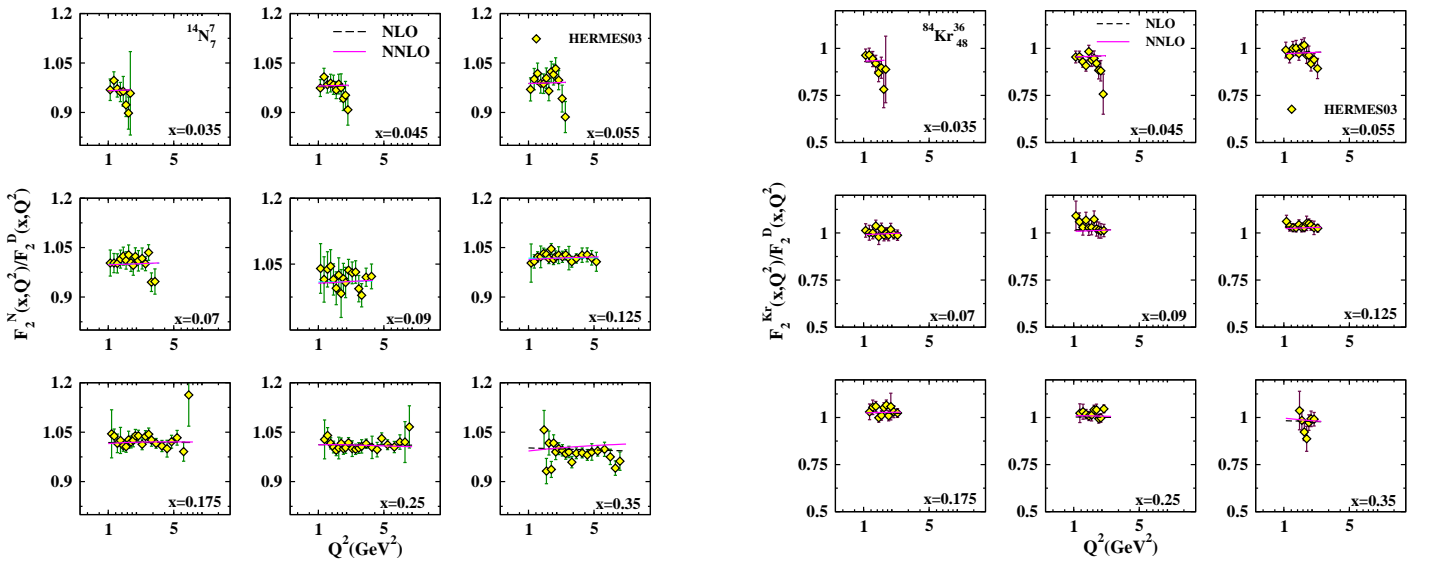
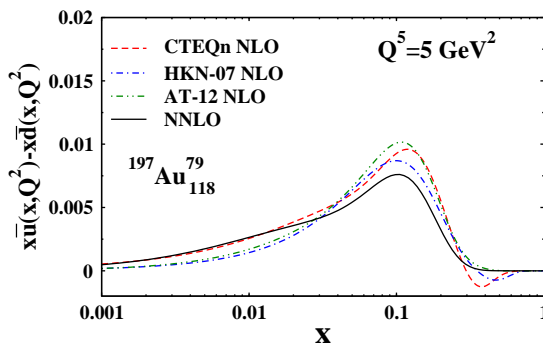
in Fig. 4 our theoretical results with the related DIS data. In Fig. 5 we show the EMC effect with uncertainties and compare with experimental data in  $Q^2 = 5 \text{ GeV}^2$ . In Fig. 6 we compare the theoretical model in  $Q^2 = 5, 10$  in NNLO, plot NLO approximation [33] and compare them with experimental data. We get good result and better than NLO approximation. In Figs 7 and 8, we depict the ratios of  $F_2^{Sn}/F_2^D$ ,  $F_2^{Kr}/F_2^D$  and  $F_2^N/F_2^C$  with respect to  $Q^2$  values and compare them with the available experimental data [21, 22] in NLO and NNLO approximation. The nuclear parton distribution functions and their uncertainties are determined by analyzing the  $F_2$  and Drell-Yan experimental data. The uncertainties are again estimated by the Hessian method.

Flavor symmetry in nuclei such as  $^2\text{D}$ ,  $^4\text{He}$ ,  $^{12}\text{C}$  and  $^{40}\text{Ca}$  are like each other in which  $\bar{u} = \bar{d} = s$ . For another nuclei that the number of their protons and neutrons are not equal, we have the  $SU(3)$  flavor symmetry breaking. We compare our model with assumption  $\bar{u} \neq \bar{d} \neq s$  with respect to HKN-07 [29], n-CTEQ [43] and AT-12 [33] results. This analysis has been done for Gold in Fig. 9 at  $Q^2 = 5 \text{ GeV}^2$  in which we have  $SU(3)$  symmetry breaking. In the first step 20 parameters have been optimized by minimizing the  $\chi^2$  value and in the second one since we fixed three parameters  $\beta_v$ ,  $\beta_{\bar{q}A}$  and  $\beta_g$ , we just need to determine 17 parameters of the weight functions via our fitting procedure. The reason that we have to fix these three parameters is that to control the fermi motions of the partons inside the nuclei at the large values of  $x$ . For the weight functions of the valance and sea quark distributions, we choose an A-dependent function while the weight function for the gluon distribution is assumed independent of A number. The numerical values in Table. 2, are listed on this base. The parameters  $a_{u_v}$ ,  $a_{d_v}$  and  $a_g$  are fixed by the three sum rules, given by Eq. (5).

If we intend to discuss about this analysis at some small enough value of  $x$  the number of gluons distributions is negative and we have saturation condition in  $Q_0^2$  for small  $x$  values. Does this mean there are no gluons in that region? No, it means we are in saturation region [44] in nuclei where overlapping of gluons with smaller impact parameter is increased. It is due to the increasing number of nucleons along a straight line. Consequently the probability for gluon recombination effects inside the nucleus would be increased [45]. This leads to gluon saturation and negative behavior at low  $x$  region. We should also notice that the small- $x$  behavior of singlet NNLO splitting functions is negative for small values of  $Q^2$  at low  $x$  region [46, 47]. The negative distribution for gluon in low  $Q^2$  shows that we have saturation condition that is very important for nuclei-nuclei collisions and for studying the quark-gluon plasma condition that occurs in the Big-bang or in the neutrons stars. In high-energy  $AA$  collisions, hard or semi-hard parton scattering in the initial stage may result in a large amount of jet production. In particular, the multiple minijets whose typical transverse moment is a few GeV could give rise to an important fraction of the transverse energy produced in the heavy ion collisions [48, 49] in the RHIC and LHC.

$a_v$	$a_{\bar{q}}$	$a_g$
Appendix A	$(-0.176 \pm 5.78 \times 10^{-3})A^{0.123 \times 10^{-2} \pm}$	Appendix
$b_v$	$b_{\bar{q}}$	$b_g$
$(2.052 \pm 2.58 \times 10^{-2})A^{-1.89 \times 10^{-2} \pm 2.91 \times 10^{-3}}$	$(3.82 \pm 8.09 \times 10^{-2})A^{0.128 \pm 3.91 \times 10^{-3}}$	$570.3 \pm 58.5$
$c_v$	$c_{\bar{q}}$	$c_g$
$(-6.769 \pm 3.68 \times 10^{-2})A^{-1.17 \times 10^{-2} \pm 1.29 \times 10^{-3}}$	$(-18.11 \pm 0.41)A^{0.145 \pm 4.63 \times 10^{-3}}$	$-2575.5 \pm 271.2$
$d_v$	$d_{\bar{q}}$	$d_g$
$(5.165 \pm 3.63 \times 10^{-2})A^{3.613 \times 10^{-3} \pm 1.78 \times 10^{-3}}$	$(16.12 \pm 0.887)A^{0.239 \pm 9.54 \times 10^{-3}}$	$2985.03 \pm 437.7$
$\beta_v$	$\beta_{\bar{q}}$	$\beta_g$
0.4 Fixed	0.1 Fixed	0.1 Fixed

Table 2. Parameters obtained by analyzing the weight functions for valance quark, sea quark and gluon distributions .

Fig. 8.  $Q^2$  dependence of  $F_2^{Kr}/F_2^D$  and  $F_2^N/F_2^D$  [21] in comparison with the results of NLO and NNLO approximations [33].Fig. 9. Flavor symmetry  $x\bar{u} - x\bar{d}$  in Gold a at  $Q^2=5 \text{ GeV}^2$  and its comparison with HKN-07[29],n-CTEQ[43] and [33] results.

## Appendix A

Having three sum rules which give us the nuclear charge  $Z$ , baryon number  $A$  and momentum conservation as in

Eq.(5), we can calculate the three parameters  $a_{uv}(A, Z)$ ,  $a_{dv}(A, Z)$  and  $a_g(A, Z)$ :

$$\begin{aligned}
 a_{uv}(A, Z) &= -\frac{ZI_1(A) + (A-z)I_2(A)}{ZI_3 + (A-Z)I_4}, \\
 a_{dv}(A, Z) &= -\frac{ZI_2(A) + (A-z)I_1(A)}{ZI_4 + (A-Z)I_3}, \\
 a_g(A, Z) &= -\frac{1}{I_8} \left\{ a_{uv}(A, Z) \left[ \frac{Z}{A}I_5 + \left(1 - \frac{Z}{A}\right)I_6 \right] \right. \\
 &\quad \left. + a_{dv}(A, Z) \left[ \frac{Z}{A}I_6 + \left(1 - \frac{Z}{A}\right)I_5 \right] + I_7(A) \right\}. \quad (10)
 \end{aligned}$$

To obtain the numerical values for these parameters in any nuclei, we need to calculate the following integrals [29]:

$$\begin{aligned}
 I_1(A) &= \int \frac{H_v(x, A)}{(1-x)^{\beta_v}} u_v(x) dx, \\
 I_2(A) &= \int \frac{H_v(x, A)}{(1-x)^{\beta_v}} d_v(x) dx,
 \end{aligned}$$



$$\begin{aligned}
I_3 &= \int \frac{1}{(1-x)^{\beta_v}} u_v(x) dx, \\
I_4 &= \int \frac{1}{(1-x)^{\beta_v}} d_v(x) dx, \\
I_5 &= \int \frac{x}{(1-x)^{\beta_v}} u_v(x) dx, \\
I_6 &= \int \frac{x}{(1-x)^{\beta_v}} d_v(x) dx, \\
I_7(A) &= \int x \left[ \frac{H_v(x, A)}{(1-x)^{\beta_v}} \{u_v(x) + d_v(x)\} \right. \\
&\quad + \frac{a_{\bar{q}}(A) + H_{\bar{q}}(x, A)}{(1-x)^{\beta_{\bar{q}}}} 2\{\bar{u}(x) + \bar{d}(x) + \bar{s}(x)\} \\
&\quad \left. + \frac{H_g(x, A)}{(1-x)^{\beta_g}} g(x) \right] dx, \\
I_8 &= \int \frac{x}{(1-x)^{\beta_g}} g(x) dx, \tag{11}
\end{aligned}$$

where  $\beta_v = 0.4$ ,  $\beta_{\bar{q}} = \beta_g = 0.1$  and  $H_i(x, A)$  is given by

$$\begin{aligned}
H_v(x, A) &= b_v(A)x + c_v(A)x^2 + d_v(A)x^3, \\
H_{\bar{q}}(x, A) &= b_{\bar{q}}(A)x + c_{\bar{q}}(A)x^2 + d_{\bar{q}}(A)x^3, \\
H_g(x) &= b_g + c_g x^2 + d_g x^3. \tag{12}
\end{aligned}$$

The results of the eight integrals in above, depend on the atomic number and are different for each nuclei.

## Appendix B

The FORTRAN package containing our unpolarized structure functions,  $F_2^A(x, Q^2)$ , for nuclei, as well as the unpolarized parton densities  $xu_v^A(x, Q^2)$ ,  $xd_v^A(x, Q^2)$ ,  $xs^A(x, Q^2)$ ,  $x\bar{u}^A(x, Q^2)$ ,  $x\bar{d}^A(x, Q^2)$ ,  $xg^A(x, Q^2)$  and their uncertainties at NNLO approximation in the  $\overline{\text{MS}}$ -scheme can be obtained via e-mail from the author. In this package we assumed  $10^{-4} \leq x \leq 0.999$  and  $2 \leq Q^2 \leq 10^5 \text{ GeV}^2$ .

## References

1. J. J. Aubert *et al.* [European Muon Collaboration], Phys. Lett. B **123** (1983) 275.
2. D. G. Yakovlev, A. D. Kaminker, O. Y. Gnedin and P. Haensel, Phys. Rept. **354** (2001) 1
3. M. Jacob and J. Tran Thanh Van, Phys. Rept. **88** (1982) 325.
4. W. Zhu, J. Ruan and F. Hou, Int. J. Mod. Phys. E **22** (2013) 1350013
5. P. Braun-Munzinger, J. Stachel, Nature **448** (2007) 302.
6. P. Amaudruz *et al.* [New Muon Collaboration], Nucl. Phys. B **441** (1995) 3.
7. J. Gomez, R. G. Arnold, P. E. Bosted, C. C. Chang, A. T. Katramatou, G. G. Petratos, A. A. Rahbar and S. E. Rock *et al.*, Phys. Rev. D **49** (1994) 4348.
8. A. Bodek, N. Giokaris, W. B. Atwood, D. H. Coward, D. L. Dubin, M. Breidenbach, J. E. Elias and J. I. Friedman *et al.*, Phys. Rev. Lett. **51** (1983) 534.
9. A. Bodek, N. Giokaris, W. B. Atwood, D. H. Coward, D. Sherden, D. L. Dubin, J. E. Elias and J. I. Friedman *et al.*, Phys. Rev. Lett. **50** (1983) 1431.
10. S. Dasu, P. de Barbaro, A. Bodek, H. Harada, M. W. Krasny, K. Lang, E. M. Riordan and R. Arnold *et al.*, Phys. Rev. Lett. **60** (1988) 2591.
11. A. C. Benvenuti *et al.* [BCDMS Collaboration], Phys. Lett. B **189** (1987) 483.
12. J. Ashman *et al.* [European Muon Collaboration], Z. Phys. C **57** (1993) 211.
13. J. Ashman *et al.* [European Muon Collaboration], Phys. Lett. B **202** (1988) 603.
14. M. R. Adams *et al.* [E665 Collaboration], Phys. Rev. Lett. **68** (1992) 3266.
15. M. R. Adams *et al.* [E665 Collaboration], Z. Phys. C **67** (1995) 403.
16. J. Seely, A. Daniel, D. Gaskell, J. Arrington, N. Fomin, P. Solvignon, R. Asaturyan and F. Benmokhtar *et al.*, Phys. Rev. Lett. **103** (2009) 202301.
17. M. Arneodo *et al.* [New Muon Collaboration], Nucl. Phys. B **441** (1995) 12.
18. M. Arneodo *et al.* [European Muon Collaboration], Nucl. Phys. B **333** (1990) 1.
19. G. Bari *et al.* [BCDMS Collaboration], Phys. Lett. B **163** (1985) 282.
20. M. Arneodo *et al.* [New Muon Collaboration], Nucl. Phys. B **481** (1996) 3.
21. M. Arneodo *et al.* [New Muon Collaboration], Nucl. Phys. B **481** (1996) 23.
22. K. Ackerstaff *et al.* [HERMES Collaboration], Phys. Lett. B **475** (2000) 386. [Erratum-ibid. B **567** (2003) 339]
23. M. A. Vasilev *et al.* [FNAL E866 and NuSea Collaborations], Phys. Rev. Lett. **83** (1999) 2304.
24. D. M. Alde, H. W. Baer, T. A. Carey, G. T. Garvey, A. Klein, C. Lee, M. J. Leitch and J. W. Lillberg *et al.*, Phys. Rev. Lett. **64** (1990) 2479.
25. A. Vogt, Comput. Phys. Commun. **170** (2005) 65.
26. P. Jimenez-Delgado and E. Reya, Phys. Rev. D **79** (2009) 074023.
27. M. Hirai, S. Kumano and M. Miyama, Phys. Rev. D **64** (2001) 034003.
28. M. Hirai, S. Kumano and T. -H. Nagai, Phys. Rev. C **70** (2004) 044905.



29. M. Hirai, S. Kumano and T. -H. Nagai, Phys. Rev. C **76** (2007) 065207.
30. S. A. Tehrani, A. N. Khorramian and A. Mirjalili, Int. J. Mod. Phys. A **20** (2005) 1927.
31. S. A. Tehrani, A. Mirjalili and A. N. Khorramian, “EMC effect and nuclear structure functions,”
32. S. A. Tehrani and A. N. Khorramian, eConf C **070910** (2007) 205.
33. S. Atashbar Tehrani, Phys. Rev. C **86** (2012) 064301.
34. S. Kumano, Phys. Rept. **303** (1998) 183.
35. G. T. Garvey and J. -C. Peng, Prog. Part. Nucl. Phys. **47** (2001) 203.
36. A. Kusina, T. Stavreva, S. Berge, F. I. Olness, I. Schienbein, K. Kovarik, T. Jezo and J. Y. Yu *et al.*, Phys. Rev. D **85** (2012) 094028.
37. I. Sick and D. Day, Phys. Lett. B **274** (1992) 16.
38. “Evidence for enhancement of gluon and valence quark distributions in nuclei from hard lepton nucleus processes,” Phys. Rev. Lett. **65** (1990) 1725.
39. F. James, CERN Program Library Long Writeup D506 (1994).
40. M. Gluck, E. Reya and A. Vogt, Z. Phys. C **48** (1990) 471.
41. W. L. van Neerven and A. Vogt, Nucl. Phys. B **568** (2000) 263.
42. W. L. van Neerven and A. Vogt, Nucl. Phys. B **588** (2000) 345.
43. I. Schienbein, J. Y. Yu, K. Kovarik, C. Keppel, J. G. Morfin, F. Olness and J. F. Owens, Phys. Rev. D **80** (2009) 094004.
44. D. G. d’Enterria, Eur. Phys. J. A **31** (2007) 816.
45. M. Chiu, 20th International Workshop on Deep-Inelastic Scattering and Related Subjects (DIS 2012) arXiv:1210.2439 [nucl-ex].
46. A. Vogt, S. Moch and J. A. M. Vermaseren, Nucl. Phys. B **691** (2004) 129.
47. A. Vogt, S. Moch and J. Vermaseren, Nucl. Phys. Proc. Suppl. **152** (2006) 110. [hep-ph/0407321]. Phys. Lett. B **189** (1987) 483.
48. K. Kajantie, P. V. Landshoff and J. Lindfors, Phys. Rev. Lett. **59** (1987) 2527.
49. K. J. Eskola, K. Kajantie and J. Lindfors, Nucl. Phys. B **323** (1989) 37.